International Journal of the Physical Sciences Vol. 6(5), pp. 948-961, 4 March, 2011
Available online at http://www.academicjournals.org/IJPS
DOI: 10.5897/IJPS10.222
ISSN 1992 - 1950 ©2011 Academic Journals

Full Length Research Paper

Flexural response of reinforced concrete members strengthened with near-surfaced-mounted CFRP strips

Ki Nam Hong[1]*, Jae Won Han[1], Dong Woo Seo[2] and Sang Hoon Han[1]

[1]Department of Civil Engineering, Chungbuk National University, Cheongju, South Korea.
[2]Department of Civil and Environmental Engineering, Northeastern University, Boston, MA 02115, USA.

Accepted 10 January, 2011

Tests and analyses were performed in this study to assess the flexural strengthening capacity of reinforced concrete (RC) members strengthened by the near surface mounted (NSM) technique, which is drawing attention as an alternative to the carbon fiber reinforced polymer (CFRP) bonding strengthening technique. Four-point bending tests were performed on 14 RC specimens. The test variables such as section geometry (250×400 and 400×200 mm), the compressive strength of concrete (27 and 34 MPa), tensile reinforcing bar ratio (0.43, 0.68, 0.98 and 1.42%), and a number of CFRP strips (one, two and three lines) were considered. Through the testing scenarios, the effect of each test variable on the failure mode and the flexural strengthening capacity of the RC members strengthened by the NSM technique were assessed. The test results show that the RC members strengthened by the NSM technique go to failure as a result of the partial CFRP fracture accompanied by crushing of the concrete in the compression zone, and that the CFRP reinforcement area as well as the section geometry have the greatest effect on the strengthening capacity. In addition, analyses confirm that the flexural strength prediction equation proposed by Yost et al.(2007) and the finite element method (FEM) analysis model proposed in this study appropriately predict the flexural strength and the load-displacement response of the RC members strengthened by the NSM technique, respectively.

Key words: Near surface mounted (NSM) technique, flexural strengthening capacity, carbon fiber reinforced polymer (CFRP) strip, four-point bending test.

INTRODUCTION

Since the development of reinforced and prestressed concrete, reinforcement bars and tendons were used for a long time as the strengthening material of concrete structures because of their economic and mechanical advantages. However recently in many countries around the world, the serviceability and safety deterioration of an SOC infrastructure caused by the corrosion of the reinforcement bar and tendon has been emerged as a new social problem. Therefore, the application of fiber reinforced polymer (FRP) in the construction field is attracting high interest as a solution to this problem. FRP as a material has the advantages of being non-corrosive, light, of high tensile strength, and a non-conductor of electricity. Moreover, it has excellent malleability and can be formed into various shapes. Recognizing the high utilization possibility and tremendous potential marketability of FRP, Japan, Europe, the US and other advanced nations have lately vested much interest and effort not only in the FRB material industry but also in its related application and technological development. The CFRP bonding strengthening technique of attaching fiber sheets or FRP plates on the tensile face of the concrete, most widely used as the technique to strengthen aged concrete structures, is currently the technique used for increasing a structure's bearing capacity. However, incidences of intermediate flexural crack-induced

*Corresponding author. E-mail: hong@chungbuk.ac.kr.

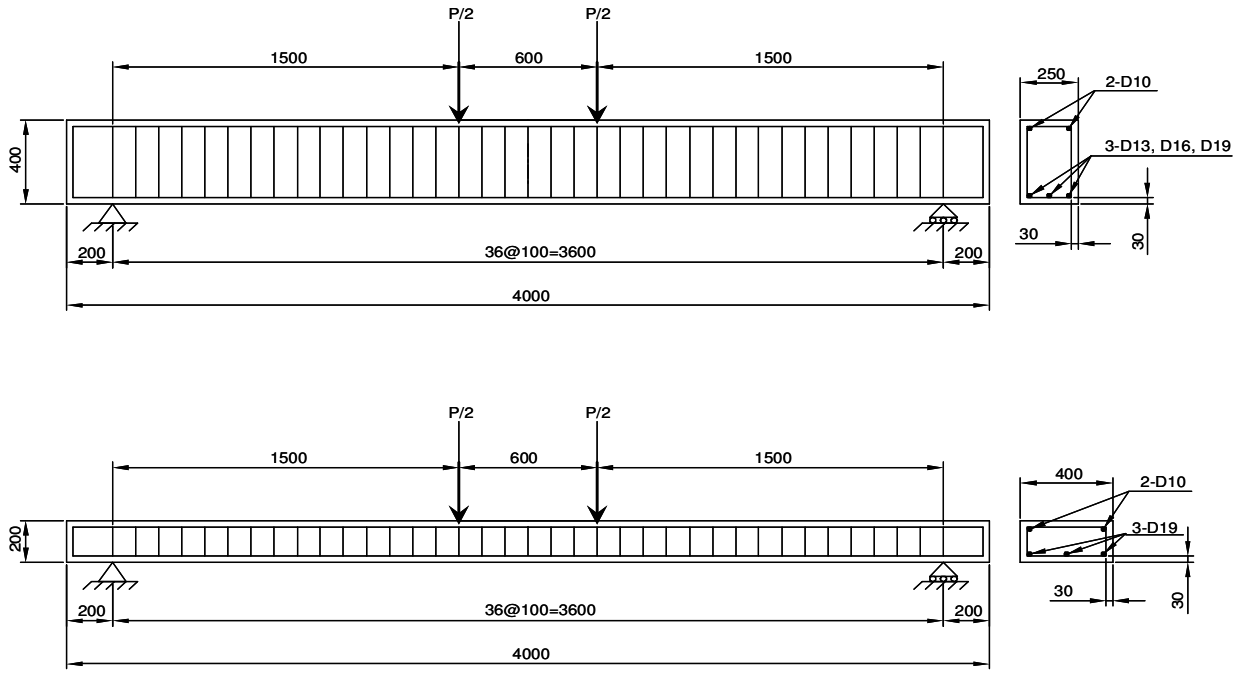

Figure 1. Details of specimens.

debonding failure, in which the strengthening material comes off of the concrete before reaching the ultimate load after the strengthening, and plate-end debonding failure caused by stress concentration at a plate's end, are being reported by many researchers (Ehsani et al., 1993; Malek et al., 1998). According to the literature previously presented, specimens strengthened by carbon fiber or glass fiber are reported to display only about 20 to 50% of the full performance capacity of the strengthening material (Chen and Teng, 2001; Teng et al., 2003).

In addition, after the strengthening, serious strengthening performance deterioration can be brought about by the risk of fire and physical damage from collision, as the FRP strengthening material is exposed to those during the stress transmission process. To resolve this problem, the near surface mounted (NSM) technique is proposed as a new alternative where a fixed-size groove is cut on the tensile side of the damaged reinforced concrete structure and the FRB strengthening material is inserted in the concrete surface so that it can behave as one body with the structure (Hassan and Rizkalla, 2003; El-Hacha and Rizkalla, 2004; Hassen and Rizkalla, 2004; Novidis et al., 2007; Taljsten et al., 2003). By inserting the strengthening material inside the concrete, the NSM technique can more effectively resolve the premature failure of the CFRP bonding strengthening technique and lower the possibility of damage from the external environment.

Currently, various test studies are being actively carried out with Europe leading the way, not only on the flexural behavior but also on the shear behavior and the bonding mechanism of the NSM strengthened reinforced concrete members (Oehlers et al., 2007; Oehlers et al., 2008; De Lorenzis, 2000; De Lorenzis et al., 2004; Mohamed Ali et al., 2008; Seracino et al., 2007). However, the design code for the RC beams strengthened by the NSM technique has yet to be established. Yost et al. (2007) asserts the need for a test study on the wide range of design variables in order to establish the design standard for this technique.

Therefore, in this study, tests were performed by selecting as the main test variables the amount of steel and CFRP reinforcement that have the greatest effect on the flexural behavior of the RC members strengthened by the NSM technique. Then we proposed a finite element method (FEM) analysis model that can accurately predict such behavior. The study results presented in this paper can be effectively utilized in establishing the design standard and assessing the performance of the NSM technique.

EXPERIMENTAL PROGRAM

Specimen configuration

To assess the effect of test variables on the flexural strengthening capacity of RC beams strengthened by the NSM technique with CFRP strips, a total of 14 specimens were designed in this study. There are two specimen section geometries, 250×400 and 400×200 mm, as shown in Figure 1. Regardless of the section geometry,

Table 1. Test variables.

Specimen	Cross-section size (mm)	Concrete compressive strength (MPa)	Reinforcing bar ratio (%)	Number of CFRP strip
ALII	250 × 400	27	0.68	-
ALII-2		27	0.68	2
AMI		34	0.43	-
AMI-2		34	0.43	2
AMII		34	0.68	-
AMII-2		34	0.68	2
AMIII		34	0.98	-
AMIII-1		34	0.98	1
AMIII-2		34	0.98	2
AMIII-3		34	0.98	3
BMIV	400 × 200	34	1.42	-
BMIV-1		34	1.42	1
BMIV-2		34	1.42	2
BMIV-3		34	1.42	3

A L II - 2
① ② ③ ④

①	Section dimension, b × h (A = 250 × 400 mm, B = 400 × 200 mm)
②	Concrete compressive strength, $f_c^{'}$ (MPa) (L = 27, M = 34)
③	Reinforcing bar ratio, (I=0.43%, II = 0.68%, III = 0.98%, IV = 1.42%)
④	Number of CFRP strip (1 = one line, 2 = two lines, 3 = three lines)

Table 2. Mixing properties of concrete.

Design strength (MPa)	Slump (cm)	Air content (%)	W/B (%)	S/a (%)	Specific weight (kg/m^3)					
					W	C	S	G	FA	AD
21.0	15.0	4.5	53	49	169	287	863	916	32	1.92
27.0	15.0	4.5	47	49	166	319	852	904	35	2.12

* W: Water, C: Cement, S: Sand, G: Gravel, FA: Fly ash, AD: Admixture.

the length and net span of all specimens are 4,000 and 3,600 mm, respectively. The length of CFRP strip is the same for all specimens, at 2,880 mm or 80% of the net span. To prevent shear failure from occurring prior to flexural failure, stirrups with a diameter of 9.53 mm were placed close together at intervals of 100 mm in all specimens. The concrete cover is 30 mm for all specimens, and 3 steel bars satisfying the tensile reinforcing bar ratio variable of each specimen were placed as the reinforcement.

Test variables

The test variables are section geometry, concrete compressive strength, tensile reinforcing bar ratio and a number of CFRP strips. The ranges of the test variables are shown in Table 1. The specimen names indicate in the order of section geometry (that is, A: 250 × 400 mm, and B: 400 × 200 mm), the concrete compressive strength (that is, L: 27 MPa, and M: 34 MPa), the tensile reinforcing bar ratio (that is, I = 0.43%, II = 0.68%, III = 0.98%, and IV = 1.42%) and the number of CFRP strips (that is, 1: 1 line, 2: 2 line, and 3: 3 line).

Materials

The maximum aggregate size of concrete used in producing the specimens is 25 mm, and the mixing design is as shown in Table 2. Simultaneously with casting of the concrete, three Ø100 × 200 mm cylinders were produced from concrete at each batch. After 28 days, the concrete compressive strength was determined through compression tests on these cylinders. The reinforcing bars used are deformed bars with nominal diameters of 9.53, 12.7, 15.9 and 19.1

Table 3. Material properties of steel bars.

No.	Nominal diameter (mm)	Modulus of elasticity (MPa)	Tensile strength (MPa)	Yield strength (MPa)	Elongation (%)
D10	9.53	2×10^5	615	533	17.1
D13	12.7		628	525	18.5
D16	15.9		631	528	16.6
D19	19.1		629	512	16.3

Table 4. Material properties of CFRP strip.

Elastic modulus	165,000 MPa
Tensile strength	2850±150 MPa
Ultimate strain	1.4%
Fiber contents	63.4%

Table 5. Material properties of epoxy.

Compressive strength	80.3 MPa
Flexural strength	42.4 MPa
Bond strength	3.0 MPa
Hardness	84 HDD

(a) (b)

Figure 2. Specimen preparation (a) groove cutting, and (b) CFRP strips after grouting.

mm. As for the tensile reinforcement, bars with diameters of 12.7, 15.9 and 19.1 mm were used. For the compressive and shear reinforcement, 9.53 mm diameter bars were used equally in all specimens. The mechanical properties of the reinforcing bars with each diameter determined by the tensile testing are given in Table 3.

The CFRP strip has a square section 10 mm wide and 2.8 mm thick. The modulus of elasticity, tensile strength, ultimate strain and fiber mixing ratio of the CFRP strip provided by the manufacturer, as shown in Table 4, are 165 GPa, 2850±150 MPa, 1.4%, and 63.4%, respectively. For the epoxy to fill the groove, the product manufactured by the CFRP strip manufacturer was used; and as shown in Table 5, the compressive strength, flexural strength, bond strength and hardness of the epoxy provided by the manufacturer are 80.3, 42.4, 3.0 MPa, and 84 HDD, respectively.

Strengthening method

The NSM strengthening process and the location of the groove in the section are shown in Figures 2 and 3, respectively. To make the groove cutting work easier, the specimen cured for 28 days was

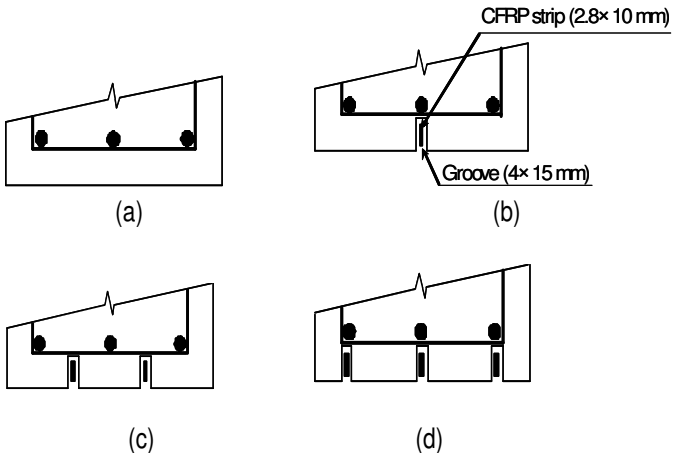

Figure 3. Location of the groove (a) control, (b) one strip, (c) two strips, and (d) three strips.

Figure 4. Test setup.

rotated 180° and the groove was cut, as shown in Figure 2(a), by using a concrete cutting device. The blade of the cutter was adjusted to fix the width and the depth of the groove to be 4 and 15 mm each, and the length of the groove was set at 2,880 mm which is 80% of the net span. With the Figure 3a control specimen as the standard, the groove of the specimen strengthened by one CFRP strip line was cut below the center tensile reinforcing bar, as shown in Figure 3b. The grooves of the specimen strengthened by two CFRP strip lines were cut in the middle location between the center reinforcing bar and the tensile reinforcing bars on both ends, as shown in Figure 3c. In addition, the grooves of the specimen strengthened by three CFRP strip lines were respectively formed below each tensile reinforcing bar, as shown in Figure 3d. The dust on the surface and in the groove of the specimens with groove cutting completed was fully removed by using an air compressor. The NSM strengthening was done in the order of filling 2/3 of the groove with epoxy, inserting the CFRP strip in the groove and then doing the surface treatment. The form of the specimen with the strengthening work completed is shown in Figure 2b. The specimens with NSM strengthening completed were cured for 7 days, and then the flexural tests were performed.

Loading method and measurement categories

As shown in Figure 4, the specimen was simply supported and placed under a four-point loading. The load was applied by a displacement control method at a speed of 1 mm/s using hydraulic equipment with a capacity of 500 kN attached to a steel frame. The displacement occurring at the center of the specimen during each loading stage was measured by 2 LVDTs installed on the lower center sides of the member. In addition, the strains of the tensile reinforcing bar and the CFRP strip were measured with the strain gauge attached at the center of the member. The load, displacement and strain measured for each loading stage were automatically saved by the data logger. The crack formation and crack progression state occurring at each loading stage were recorded above the specimen crack. After the completion of the test, the tensile concrete zone with the greatest damage was shattered with a hammer drill and the degree of damage to the CFRP strip was examined.

TEST RESULTS

Failure mode

The final failure mode of each test specimen is determined by referring to the initiation and growth of the cracks, and values of strain gauge attached to the CFRP strips and main tensile steel bars. The final failure modes of each test specimen are shown in Table 6.

All the control specimens without strengthening reached failure by the typical flexural failure mode. In these, flexural cracks occurred in the lower side of the middle area at regular intervals during the initial loading stage. As the loading increased, these flexural cracks grew vertically toward the compression zone. As the strain of the steel bar reached the yield strain, the flexural crack in the middle of the span widened and the deflection began to increase rapidly. The AMI with the smallest tensile reinforcing bar ratio showed the typical flexural failure mode where a deflection of 50 mm or more occurs even when there is no substantial damage to the concrete in the compression zone. In contrast, the ALII, AMII, AMIII, and BMIV specimens displayed the flexural-compression failure mode, where the load is maintained for a period of time, and then when the concrete in the compression zone starts to be crushed, the deflection increases rapidly. Moreover, the failure behavior of these specimens showed that the greater the tensile reinforcing bar ratio of a specimen, the more the displacement at the point of compression failure tends to decrease.

The specimens strengthened by the NSM technique all showed similar failure behavior. Hence, the failure behavior of the specimens strengthened by the NSM technique is explained on the basis of the failure behavior

Table 6. Test results.

Specimen	P_{sy} (kN)	P_u (kN)	δ_u (mm)	$(P_u-P_{uo})/P_{uo}$ (%)	*Failure type
ALII	145.95	149.94	40.64	-	SY, CC
ALII-2	166.39	194.55	32.90	29.75	SY, CC, TR
AMI	101.00	103.10	42.82	-	SY, CC
AMI-2	111.12	146.86	33.52	42.44	SY, TR
AMII	137.32	155.34	50.04	-	SY, CC
AMII-2	160.33	196.82	34.32	26.70	SY, CC, TR
AMIII	186.44	196.00	35.14	-	SY, CC
AMIII-1	185.62	208.48	29.22	6.37	SY, CC, TR
AMIII-2	195.31	232.10	35.24	18.41	SY, CC, TR
AMIII-3	198.79	240.58	35.18	22.74	SY, CC, TR
BMIV	72.52	79.18	67.60	-	SY, CC
BMIV-1	79.03	89.02	64.92	12.40	SY, CC, TR
BMIV-2	79.03	94.78	68.34	19.70	SY, CC, TR
BMIV-3	83.11	104.92	72.30	32.51	SY, CC, TR

*SY = Steel yielding, CC = Concrete crushing, TR = CFRP tensile rupture.

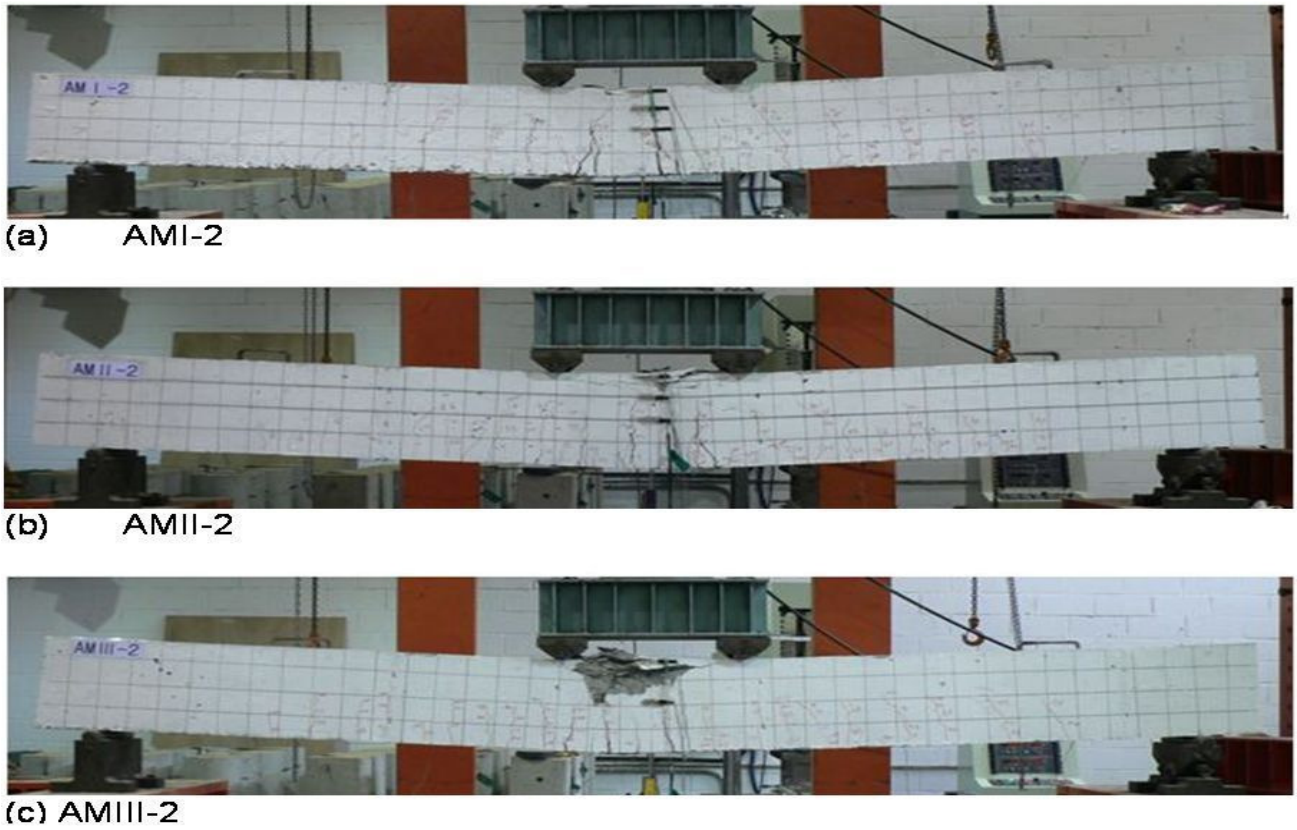

Figure 5. Failure mode.

of the AMI-2, AMII-2 and AMIII-2 specimens that are representatively shown in Figure 5. When the load passed the 50 kN mark, flexural cracks began to form from the center of the specimen at intervals of about 100 mm. When the load passed approximately 70 to 80 kN, the flexural cracks from the center region of the specimen

Figure 6. Damage of CFRP strip after testing.

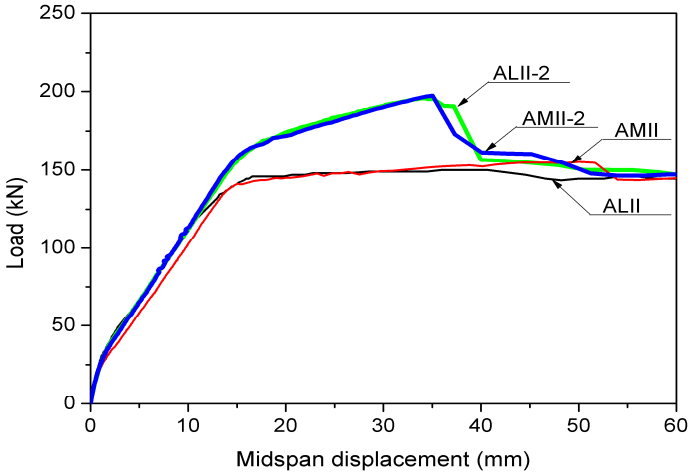

Figure 7. Comparison of load-displacement curves with respect to concrete strength.

grew vertically to about 200 mm. From this point, flexural cracks began to form in the epoxy placed in the groove at the center region of the specimen. As the steel bar yielded, the speed of load increase became very slow and the deflection began to increase rapidly. At this point, the deflection of the AMI-2 specimen with the smallest reinforcing bar ratio increased sharply with a large sound from the CFRP strip breaking, and the testing was terminated. As shown in the full view of the final failure in Figure 5a, the crushing of the concrete in the AMI-2 specimen did not occur. In all specimens except the AMI-2, as flexural crack widened, failure began from the concrete crushing. As the crushed area of the concrete increased, the deflection increased greatly, and when the CFRP plate fractured in the specimen's tensile zone with a loud noise, the testing was terminated. From the full view of the final failure shown in Figure 5, it could be confirmed that as the reinforcing bar ratio increased, the crushed area of the concrete in the compression zone substantially increased. Through an examination of specimens after the completion of all the testing, it was confirmed that no slip occurred between the CFRP strip and the concrete surface.

It was also verified that the tensile concrete damage to the AMIII-1, AMIII-2, and AMIII-3 specimens with a 250 × 400 mm section was more serious than that to the BMIV-1, BMIV-2, and BMIV-3 specimens with a 400 × 200 mm section. This is judged to be due to the smaller gap between the CFRP strips of the specimens with a 250 × 400 mm section compared with the specimens with a 400 × 200 mm section. Moreover, as shown in Figure 6, only 70 to 80% of the CFRP strips of all specimens were fractured, and the occurrence of local splitting was verified. This phenomenon is deemed to occur since the height of the CFRP strip is so large relative to its thickness, and under the flexural tension a large tensile stress difference occurs as a result of the CFRP height.

Effect of the concrete compressive strength

Figure 7 shows the load-displacement curves of the ALII-2 and AMII-2 specimens which have the same tensile reinforcing bar ratio and number of CFRP strips but different compressive strengths of 27 and 34 MPa. Figure 7 also shows the load-displacement curves of the ALII and AMII, which are control specimens of ALII-2 and AMII-2, respectively. The ALII-2 and AMII-2 specimens show the same behavior both before and after the yield of the steel bars. For the ALII-2 and AMII-2 specimens reinforced with 2 lines of CFRP strips, the load increased at the point of yielding by 45 and 41 kN, respectively, over ALII and AMII. In addition, the load continued to increase for ALII-2 and AMII-2 even after the yield of the steel bars, and then it rapidly decreased due to crushing of the concrete at the point at which the deflection for each reached 32.90 and 34.32 mm, respectively. The ultimate loads of ALII and AMII are 149.94 and 155.34 kN, respectively. In addition, the ultimate loads of ALII-2 and AMII-2, compared with the control specimens, showed load increases of 29.75 and 26.70%, respectively.

The load-CFRP strain relationships of ALII-2 and AMII-2 are shown in Figure 8. It can be confirmed through the data in Figure 8 that the strain of the CFRP strips inserted in the ALII-2 and AMII-2 specimens also showed similar behavior. The strains of the two specimens' CFRP strips began to increase after the formation of the initial crack in the tensile zone, and rapidly increased as the load burden grew after the yield of the steel bars. The

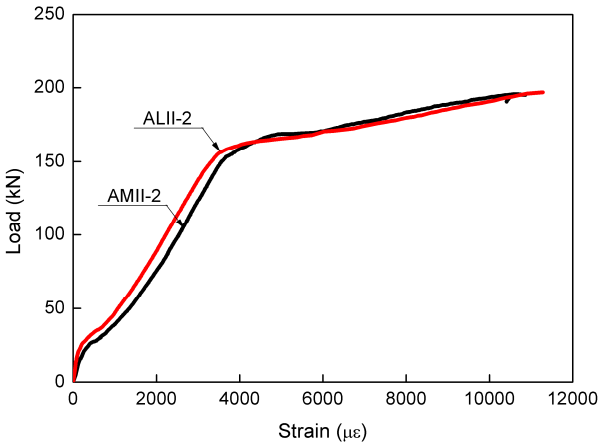

Figure 8. Comparison of load-CFRP strain curves with respect to concrete strength.

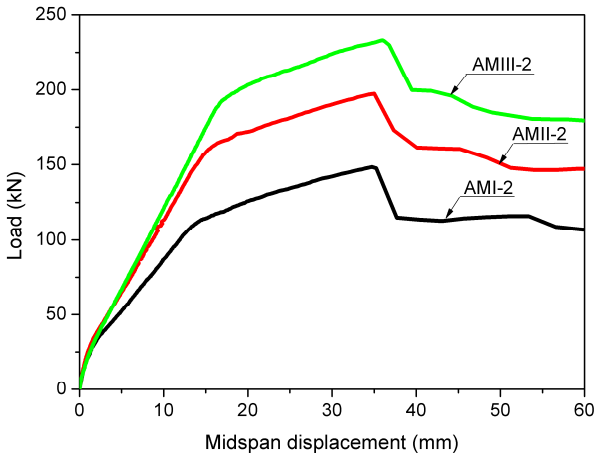

Figure 9. Comparison of load-displacement curves with respect to tensile reinforcing bar ratio.

maximum strains of the CFRP strips strengthening ALII-2 and AMII-2 are 10410 and 11285 με, respectively, and they do not show a large difference. Therefore, it can be confirmed from the results of these specimens that the effect of compressive strength on the behavior of the RC members flexurally strengthened by the NSM technique is very slight.

Effect of the tensile reinforcing bar ratio

The load-displacement curves of the AMI-2, AMII-2, and AMIII-2 specimens are shown in Figure 9. These specimens have the same compressive strength and number of CFRP strips, respectively 34 MPa and 2 lines. The tensile reinforcing bar ratios for AMI-2, AMII-2, and

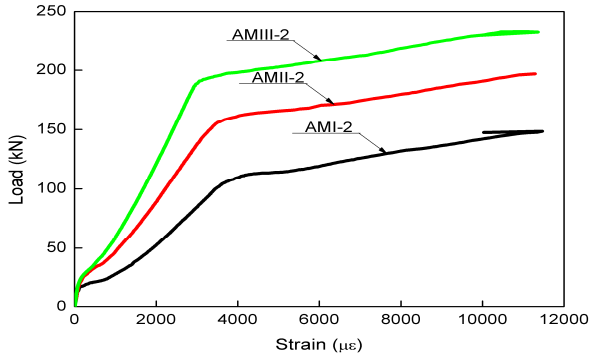

Figure 10. Comparison of load-CFRP strain curves with respect to tensile reinforcing bar ratio.

AMIII-2 are 0.43, 0.68 and 0.98%, respectively. The slope of the load-displacement curve prior to the yield of the steel bar is found to become clearly steeper as the tensile reinforcing bar ratio increases. The behavior in this section is similar to that of AMI, AMII, and AMIII, the control specimens of AMI-2, AMII-2, and AMIII-2. The slope of the load-displacement curve after the yield the steel bar is confirmed to become somewhat rapid at 1.29, 1.59 and 1.82 kN/mm for AMI-2, AMII-2, and AMIII-2, respectively, as the tensile reinforcing bar ratio increases. The ultimate loads of AMI-2, AMII-2, and AMIII-2, compared with the control specimens, increased by 42.11, 26.70 and 18.4%, respectively. That is, even if strengthening is done with the same CFRP strips, the strengthening efficiency is found to decrease as the tensile reinforcing bar ratio increases.

The load-CFRP strain relationships of AMI-2, AMII-2, and AMIII-3 are shown in Figure 10. Figure 10 shows that, regardless of the tensile reinforcing bar ratio, there is almost no occurrence of CFRP strip strain in all the specimens prior to the initial crack formation. In addition, it indicates that the smaller the tensile reinforcing bar ratio, the sharper the increase of the strain of the CFRP strip immediately after the initial crack formation. This can be predicted to occur because the load burden of the CFRP occurs earlier for a specimen with a smaller tensile reinforcing bar ratio. Under ultimate loads, the CFRP strip strains of AMI-2, AMII-2, and AMIII-3 are 10034, 11285 and 11359 με, respectively. It indicates showing that as the tensile reinforcing bar ratio increases the maximum strain of the CFRP strip increases slightly, but there is no large difference.

Effect of the number of CFRP strips and section geometry

The load-displacement curves of the AMIII, AMIII-1, AMIII-2, and AMIII-3 specimens are shown in Figure 11.

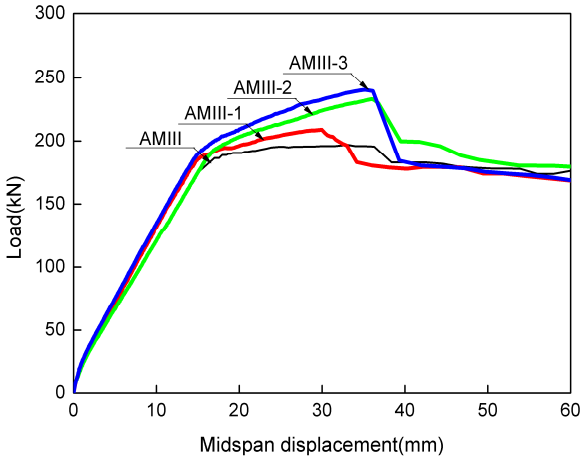

Figure 11. Comparison of load-displacement curves with respect to a number of CFRP strips (AMIII series).

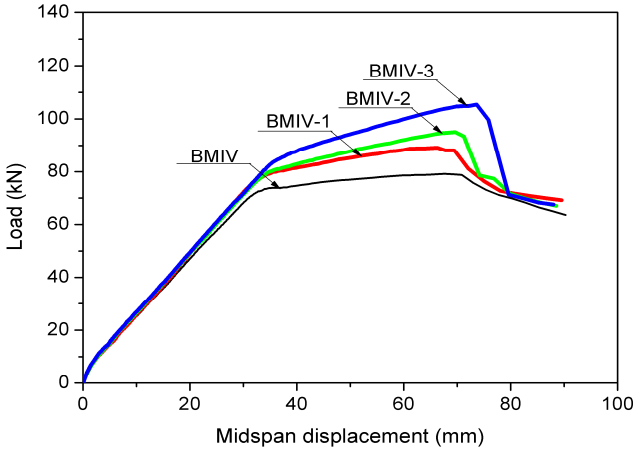

Figure 12. Comparison of load-displacement curves with respect to a number of CFRP strips (BLIV series).

These have the same section size (250 × 400 mm), compressive strength (34 MPa) and tensile reinforcing bar ratio (0.98%), but the number of CFRP strips are different at 0, 1, 2, and 3 lines, respectively, for the AMIII, AMIII-1, AMIII-2, and AMIII-3. The load-displacement curves of the BMIV, BMIV-1, BMIV-2, and BMIV-3 specimens are shown in Figure 12. These specimens also have the same section size (400 × 200 mm), compressive strength (34 MPa) and tensile reinforcing bar ratio (1.42%), but the number of CFRP strips are different at 0, 1, 2, and 3 lines, respectively, for the BMIV, BMIV-1, BMIV-2, and BMIV-3. The AMIII-1, AMIII-2, and AMIII-3 specimens in Figure 11 showed load increases of 6.37, 18.41 and 22.74%, respectively, compared with the maximum load of the AMIII. Through this, it can be

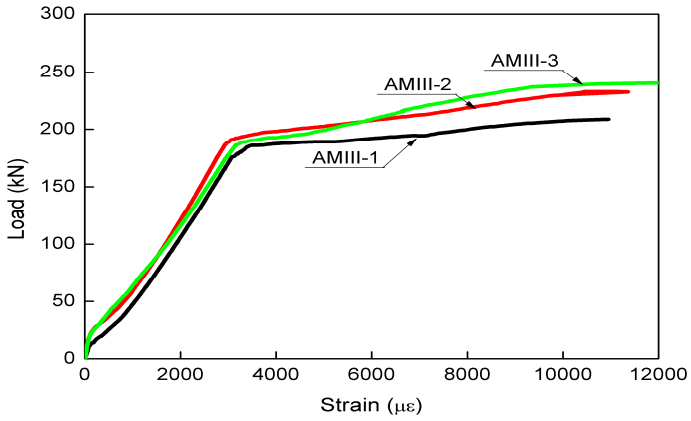

Figure 13. Comparison of load-CFRP strain curves with respect to a number of CFRP strips (AMIII series).

confirmed that the reinforcement performance does not increase linearly based on the number of strips, but tends to converge at a certain level. It is thought that since the failure is not due to the CFRP strip fracture but originates with crushing of the concrete, the strengthening efficiency is closely related to the compressive capacity of the concrete. The BMIV-1, BMIV-2 and BMIV-3 specimens in Figure 12 showed load increases of 12.40, 19.70 and 32.51%, respectively, compared with the maximum load of the BMIV. From these results, it can be confirmed that, unlike the AMIII series specimens, for the BMIV series specimens the maximum load increases proportionately to the number of CFRP strips. This is thought to be due to the larger concrete section size of the BMIV series specimens bearing the compressive force, compared with the AMIII series specimens. For the AMIII and BMIV series specimens, it was verified through Figures 11 and 12 that failure began respectively within the ranges of 30 to 35 and 65 to 72 mm, largely regardless of the number of CFRP strips. These results show that the failure for all of the AMIII and BMIV series specimens begins not from the CFRP strip fracture, but rather that the failure of the beams starts from crushing of the compression concrete.

Figures 13 and 14 show the load-CFRP strip strain relationships at the centers of the AMIII and BMIV series specimens. Figures 13 and 14 show the behavior of the CFRP strip strain for all the specimens strengthened with CFRP strips gradually increasing prior to the yield of the steel bar, and then sharply increasing after yielding. From Figure 13, the maximum CFRP strip strains of AMIII-1, AMIII-2 and AMIII-3 are confirmed to be 10953, 11359 and 12013 με, respectively. Figure 14 shows that the maximum CFRP strip strains of BMIV-1, BMIV-2, and BMIV-3 are 9873, 11702 and 11456 με, respectively. Since the ratio between the maximum CFRP strip strain determined by testing and the ultimate strain of the material is shown to average 79%, it can be confirmed

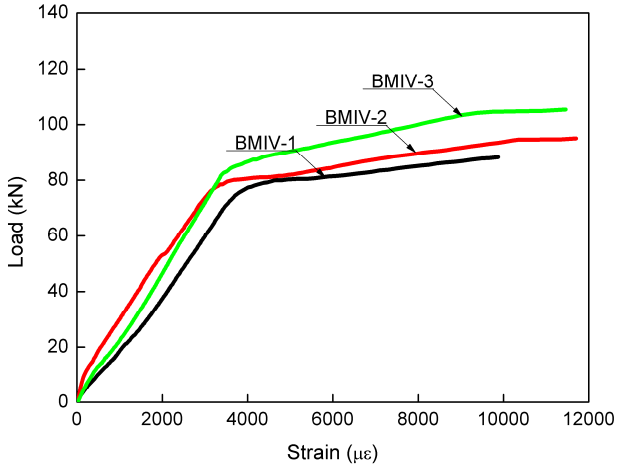

Figure 14. Comparison of load-CFRP strain curves with respect to a number of CFRP strips (BMIV series).

that the strengthening efficiency of the NSM technique is substantially superior to that of the CFRP bonding strengthening technique which display only about 20 to 50% of the full performance capacity of the strengthening material.

PREDICTION OF FLEXURAL STRENGTH

In this study, flexural strength predictions for the specimens were estimated through the flexural strength equation of the NSM strengthened RC members proposed by Yost et al. (2007), which is explained here. The failure mode of the reinforced concrete beam strengthened with FRP is determined by the area of the tensile reinforcing bar and the FRP. Equation (1) determines the balanced-strengthened area of the FRP at which the crushing of the concrete and tensile failure of the FRP can occur simultaneously.

$$A_{fb} = \frac{0.85 f_c' b \beta_1 d_f \left\{ \frac{\varepsilon_{cu}}{\varepsilon_{cu} + \varepsilon_{fu}} \right\} - A_s f_y}{f_{fu}} \quad (1)$$

where, A_{fb} = the balanced-strengthened area of the FRP, A_s = the area of the tensile reinforcing bar, f_{fu} = the ultimate stress of the FRP, f_y = yielding stress of the tensile reinforcing bar, b = the width of the section, ε_{cu} = the ultimate strain of the concrete (0.003), ε_{fu} = the ultimate strain of the FRP, and d_f = the depth of the FRP.

When the FRP area (A_f) of the beam section is smaller than the balanced-strengthened area of the FRP (A_{fb}), the tensile fracture of the FRP occurs before the occurrence of the crushing of the concrete. At such a point, nominal flexural strength of the section is calculated through Equations (2) and (3).

$$a = \frac{A_f f_{fu} + A_s f_y}{0.85 f_c' b} \quad (2)$$

$$M_n = A_f f_{fu} \left(d_f - \frac{a}{2} \right) + A_s f_f \left(d_s - \frac{a}{2} \right) \quad (3)$$

where, a = the compression block depth, M_n =the nominal moment strength, and f_c' =the concrete compressive strength. When the FRP area (A_f) of the beam section is greater than the balanced-strengthened area of the FRP (A_{fb}), the crushing of the concrete occurs before the occurrence of the tensile rupture of the FRP. If it is assumed that the steel bar yielded at the point of the occurrence of the compression failure of the concrete, the nominal flexural strength of this section can be calculated through Equations (4) through (6).

$$a = \frac{\sqrt{\left(A_f E_f \varepsilon_{cu} - A_s f_y\right)^2 + 4(0.85) f_c' b \beta_1 A_f \varepsilon_{cu} d_f}}{2(0.85) f_c' b} - \frac{\left(A_f E_f \varepsilon_{cu} - A_s f_y\right)}{2(0.85) f_c' b} \quad (4)$$

$$f_f = E_f \varepsilon_{cu} \frac{\left(d_f - a/\beta_1\right)}{a/\beta_1} \leq f_{fu} \quad (5)$$

$$M_n = A_f f_f \left(d_f - \frac{a}{2} \right) + A_s f_y \left(d_s - \frac{a}{2} \right) \quad (6)$$

where, f_f = the actual stress of the FRP, E_f = the elastic modulus of reinforcing bar, and d_s = the effective depth of the tensile steel bar

In this study, the flexural strength prediction results for the specimens, which have been flexurally strengthened with FRP strips, are shown in Table 7. $P_{u,\,Yost}$ in Table 7 is the nominal flexural strength calculated from Equations

Table 7. Comparison of test result and analysis.

Specimen	$P_{u,test}$ (kN)	$P_{u, Yost}$ (kN)	$P_{u,test}/P_{u, Yost}$	$\varepsilon_{CFRP, test}$ (με)	$\varepsilon_{CFRP, Yost}$ (με)	$\varepsilon_{CFRP, test}/\varepsilon_{CFRP, Yost}$
ALII-2	194.6	183.7	1.06	10410	10777	0.97
AMII-2	196.8	196.0	1.00	11285	12784	0.88
AMI-2	146.9	154.0	0.95	10034	16436	0.61
AMIII-1	208.5	214.6	0.97	10953	10924	1.00
AMIII-2	232.1	231.9	1.00	11359	9859	1.15
AMIII-3	240.6	246.4	0.98	12013	9071	1.32
BMIV-1	89.0	92.5	0.96	9873	8145	1.21
BMIV-2	94.8	98.7	0.96	11702	7460	1.57
BMIV-3	104.9	103.9	1.01	11456	6931	1.65

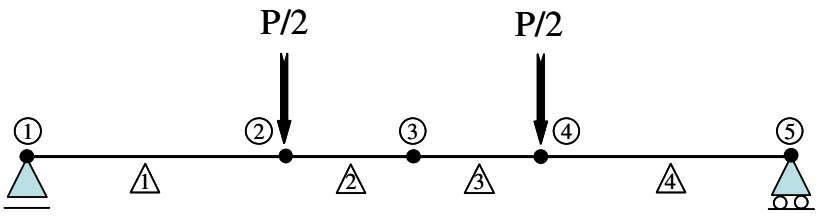

Figure 15. FE mesh for 4-point bending test.

(2) and (6) disregarding the self-weight effect and converted into the concentrated load. The mean and the standard deviation of $P_{u,test}$ /$P_{u, Yost}$, the ratio of the maximum load from the test value against the prediction equation value, shown in Table 7 are 0.99 and 0.0342, respectively. From this, it is determined that the flexural strength of the RC beams strengthened by the NSM technique can be predicted very accurately through the equation proposed by Yost et al. (2007). However, since the mean and the standard deviation of $\varepsilon_{CFRP, test}/\varepsilon_{CFRP, Yost}$, the ratio of maximum strain of the CFRP strip from the test value against the prediction equation value, are 1.15 and 0.33, respectively; the equation proposed by Yost et al.(2007) was confirmed to greatly underestimate the strain of the CFRP. This is considered to be the case because local stress concentration occurs in the CFRP strip as flexural cracks occur in the tensile zones of the NSM-strengthened specimens along with the load increase.

PREDICTION OF LOAD-DEFLECTION BEHAVIOR

To predict the load-displacement behavior of the RC beams flexurally strengthened by the NSM technique, finite element (FE) analyses using OpenSees (2006) were performed in this study. The analysis model, as shown in Figure 15, was constructed to depict a four-point bending test. This analysis model consists of 5 nodes and 4 supplementary member elements. Used as the supplementary element was the dispBeamColumn element, a displacement-based Beam-column element that has superior convergence and can be applied to a fiber section model. For each element, five integration points were equally selected. The section of the member element was modeled by using a fiber section model. In the fiber section model, the concrete, as shown in Figure 16, was divided into 8 equal parts in the width direction and 16 equal parts in the height direction. The reinforcing bar and the CFRP strip were modeled with the identical conditions of each specimen. The one-dimensional models of the concrete, reinforcing bar and CFRP strip applied to the fiber section model are given in Figures 17 to 19. For the concrete, the Concrete02 material model of Figure 17 provided by OpenSees (2006) was used. The tensile behavior of concrete is considered as linear tension softening in the Concrete02 material model. For the reinforcing bar, the Steel02 material model of OpenSees (2006) shown in Figure 18 was used. This model is based on the Menegotto-Pinto (1973) material model. As shown in Figure 19, the CFRP strip was modeled by combining the uniaxialMaterial and MinMax material models of OpenSees in order to have the elastic-brittle behavior only in the tensile zone. The bonding between the CRFP strip and the concrete was assumed to be perfect.

The nonlinear FE analyses were performed using an incremental displacement-controlled technique based on

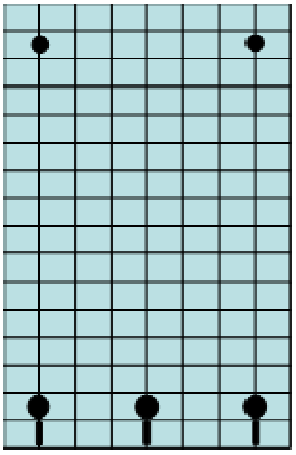

Figure 16. Fiber discretization of cross-section.

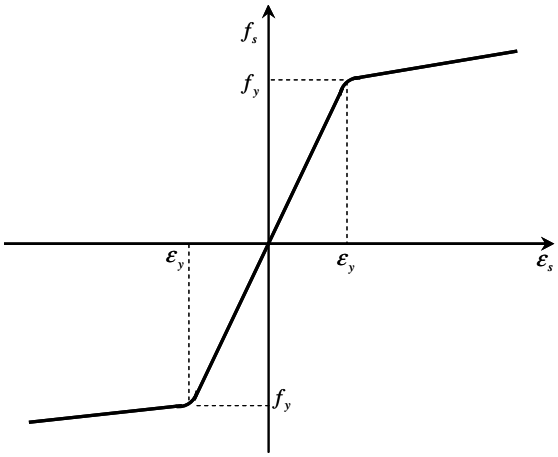

Figure 18. Steel material constitutive model.

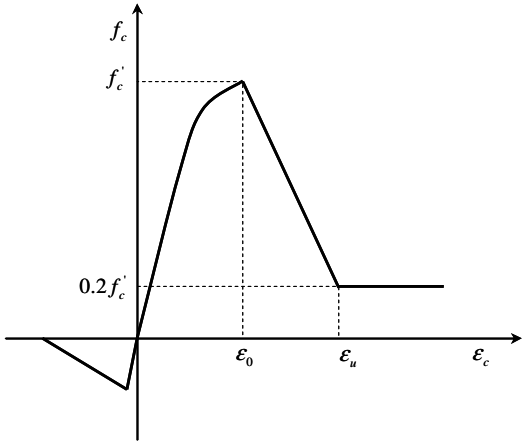

Figure 17. Concrete material constitutive model.

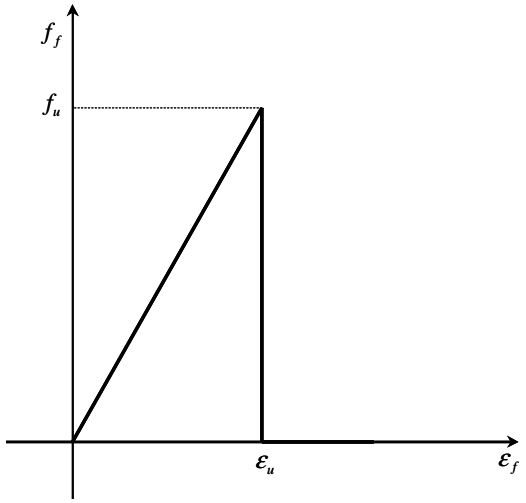

Figure 19. CFRP material constitutive model.

a Newton–Raphson iterative procedure in which vertical displacement is applied at the loading points and the internal resisting force is computed. The analyses were performed by increasing the displacement by 0.001 mm increments until the vertical displacements of the 250 × 400 and 400 × 200 mm size specimens reached 60 and 80 mm, respectively.

The comparison of nonlinear FE analysis results and test results on the load-displacement response is shown in Figure 20. Figure 20 shows that FE analysis results accurately predict the yield load of the steel bar, maximum load and deflection at the point of maximum load. In particular, based on the observation that there is not much difference between the analysis results and the test results despite assuming perfect bonding between the concrete and the CFRP strip, it can be analytically confirmed that slipping does not occur between the concrete and the CFRP strip during the testing. The results also accurately predict the compression failure mode, where the load suddenly decreases with the occurrence of the concrete crushing prior to the tensile fracture of the CFRP strip.

However, for the B-type specimens BMIV-1, BMIV-2, and BMIV-3, which have a greater effect of compression concrete on the behavior of the members than the A-type specimens, the displacement at the point of maximum loading tends to appear smaller than that of the test value. This is deemed to occur because the analytical prediction of the ultimate strain of the concrete at the point of the crushing of the concrete is smaller than the

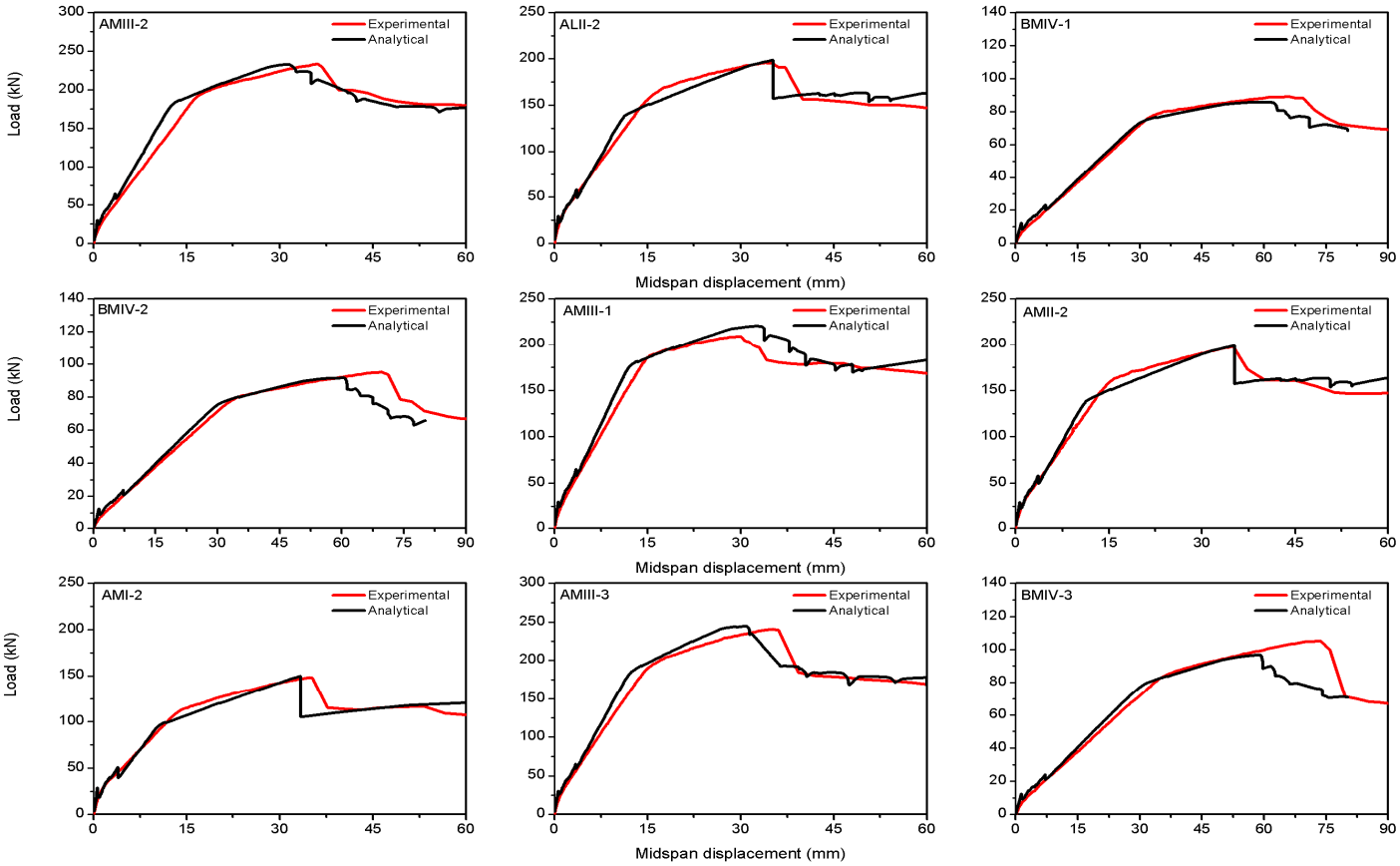

Figure 20. Comparison between experimental results and FE analysis of the load-displacement responses.

value obtained from testing. This can be resolved through a modification of the concrete material model. Therefore, it is judged that the analysis model proposed in this study can be very usefully applied in predicting the flexural behavior of RC members strengthened by the NSM technique.

Conclusions

In this study, four-point bending tests were performed on RC members flexurally strengthened with the NSM CFRP strips, and the flexural behavior of the strengthened members was analyzed based on test variables. In addition, their usefulness was examined through the flexural performance prediction equation, comparison of analysis and test results. The summary of the results derived through this study is as follows:

1. Almost all specimens flexurally strengthened by the NSM technique failed due to CFRP fracture accompanied by the concrete crushing. However, with only 70 to 80% fractures, the CFRP strips did not break completely and local area splitting occurred. This is judged to be a phenomenon occurring due to the local tensile stress difference caused by the CFRP strip having a very thin width relative to its height.
2. The effect of the concrete compressive strength on the strengthening performance of RC members flexurally strengthened by the NSM technique is not large, and the strengthening performance is shown to decrease as the tensile reinforcing bar ratio increases. The effect of the number of CFRP strips on the strengthening performance varies greatly depending on the section geometry due to the difference of the compression capacity of the concrete.
3. When the prediction equation proposed by Yost et al. (2007) was used, the flexural strength of the RC members strengthened by the NSM technique could be predicted very accurately. However, this proposed equation significantly underestimated the strain of the CFRP. This is thought to be due to the occurrence of local stress concentration in the CFRP strip resulting from the flexural cracks forming in the tensile zones of the NSM-strengthened specimens together with the load increase.
4. The FE analysis results accurately predicted the yield load of the steel bar, maximum load and deflection at the point of maximum load. In particular, based on the

observation that there was not much difference between the analysis results and the test results despite assuming perfect bonding between the concrete and the CFRP strip, it could be analytically confirmed that slipping does not occur between the concrete and the CFRP strip during the testing.

ACKNOWLEGEMENT

This research was supported by the research grant of the Chungbuk National University in 2010, and it is gratefully acknowledged.

REFERENCES

Chen JF, Teng JG (2001). Anchorage Strength Models for FRP and Steel Plates Bonded to Concrete. J. Struct. Eng. ASCE, 127(7): 784-791.

De Lorenzis L (2000). Strengthening of RC Structures with Near-Surface Mounted FRP Rods. MS Thesis. Dept. of Civ. Eng., The University of Missouri-Rolla, Rolla, MO, USA.

De Lorenzis L, Lundgren K, Rizzo A (2004). Anchorage Length of Near-Surface Mounted Fiber-Reinforced Polymer Bars for Concrete Strengthening -Experimental Investigation and Numerical Modeling. ACI Struct. J., 101(2): 269-278.

Ehsani MR, Saadatmanesh H, Tau S (1993). Bond of GFRP Rebars to Ordinary-Strength Concrete. ACI Special Pub., 1: 333-345.

El-Hacha R, Rizkalla SH (2004). Near-Surface-Mounted Fiber-Reinforced Polymer Reinforcements for Flexural Strengthening of Concrete Structures. ACI Struct. J., 101(5): 717-726.

Hassan T, Rizkalla S (2003). Investigation of Bond in Concrete Structures Strengthened with Near Surface Mounted Carbon Fiber Reinforced Polymer Strips. J. Compos. Constr., 7(3): 248-257.

Hassan TK, Rizkalla S (2004). Bond mechanism of near-surface-mounted fiber-reinforced polymer bars for flexural strengthening of concrete structures. ACI Struct. J., 101(6): 830-838.

Malek AM, Saadatmanesh H, Ehsani MR (1998). Prediction of failure load of R / C beams strengthened with FRP plate due to stress concentration at the plate end. ACI Struct. J., 95(2): 142-152.

Menegotto M, Pinto P (1973). Method of analysis for cyclically loaded reinforced concrete plane frames including changes in geometry and non-elastic behavior of elements under combined normal force and bending. IABSE symposium on resistance and ultimate deformability of structures acted on by well-defined repeated load, Zurich, Switzerland, pp. 112-123.

Mohamed AMS, Oehlers DJ, Giffith MC, Seracino R (2008). Interfacial stress transfer of near surface-mounted FRP-to- concrete joints. Eng. Struct., 30(7): 1861-1868.

Novidis D, Pantazopoulou SJ, Tentolouris E (2007). Experimental study of bond of NSM-FRP reinforcement. Constr. Build. Mater., 21(8): 1760-1770.

Oehlers DJ, Liu I, Seracino R (2007). A generic design approach for EB and NSM longitudinally plated RC beams. Constr. Build. Mater., 21(4): 697-708.

Oehlers DJ, Rashid R, Seracino R (2008). IC debonding resistance of groups of FRP NSM strips in reinforced concrete beams. Constr. Build. Mater., 22(7): 1574-1582.

OpenSees (2006). <http://opensees.berkeley.edu/index.php>.

Seracino R, Raizal Saifulnaz MR, Oehlers DJ (2007). Generic Debonding Resistance of EB and NSM Plate-to-Concrete Joints. J. Compos. Constr., 11(1): 62-70.

Taljsten B, Carolin A, Nordin H (2003). Concrete structures strengthened with near surface mounted reinforcement of CFRP. Adv. Struct. Eng., 6(3): 201-213.

Teng JG, Smith ST, Yao J, Chen JF (2003). Intermediate crack-induced debonding in RC beams and slabs. Constr. Build. Mater., 17(6): 447-462.

Yost JR, Shawn PG, David WD, Jason JM (2007). Flexural behavior of concrete beams strengthened with near-surface-mounted CFRP strips. ACI Struct. J., 104(4): 430.